Strategies for the intensification of CO_2 valorization in the one-step DME synthesis process

Ainara Ateka*, Javier Ereña, Javier Bilbao, Andrés T. Aguayo

Department of Chemical Engineering, University of the Basque Country, P.O. Box 644, 48080 Bilbao, Spain

Tel.: 34-94-6015361

* ainara.ateka@ehu.eus

ABSTRACT

The intensification of CO_2 valorization has been theoretically studied in the direct synthesis of dimethyl ether (DME) carried out in a packed-bed reactor by means of two strategies pursuing the attenuation of the thermodynamic limitations of the process. Thus, the recycling of the non-converted reactants, and the use of H_2O perm-selective membranes, with different sweeping strategies has been studied. Special attention has been paid on improving the yield of DME and the conversion of CO_2, seeking for a good balance between both objectives. The study has been conducted using the kinetic model previously established for a CuO-ZnO-MnO/SAPO-18 catalyst. Quantifying the deactivation kinetics in the kinetic model has allowed us to ascertain that both strategies contribute to attenuating deactivation. With a recirculation factor of 0.97, for a CO_2/CO_x ratio in the feed of 0.25, at 275 ºC and 30 bar, a CO_2 conversion of 70 % and a DME yield of 60 % are achieved. Using in the simulation a membrane with a H_2O permeability

of $1 \cdot 10^{-7}$ mol s^{-1} m^2 Pa^{-1} and a H_2O/H_2 selectivity of 4, feasible with H-SOD type zeolite membranes, increases CO_2 conversion up to 3.5-5 % with regard to that obtained in a packed-bed reactor, and outstands the upgrade in DME yield, reaching an improvement of 25 % for the hydrogenation of pure CO_2, regardless the sweeping strategy used (parallel or counter-current mode, or using pure H_2 or H_2+CO+CO_2).

KEYWORDS: CO_2, valorization, Dimethyl ether; Recirculation; Membrane; Bifunctional catalyst; Syngas

1. INTRODUCTION

The direct synthesis of DME has a great interest in the power to liquid context,[1] due to its excellent properties[2,3], and it is considered to be the cleanest substitute for diesel[4-7] and a promising raw material for the production of hydrocarbons (replacing methanol)[8-10] and for the production of H_2 (through steam reforming).[11,12] The reactions involved in the synthesis of DME comprise:

Methanol synthesis: $CO + 2H_2 \leftrightarrow CH_3OH$ (1)

$CO_2 + 3H_2 \leftrightarrow CH_3OH + H_2O$ (2)

Methanol dehydration to DME: $2CH_3OH \leftrightarrow CH_3OCH_3 + H_2O$ (3)

Reverse water gas shift (rWGS): $CO_2 + H_2 \leftrightarrow CO + H_2O$ (4)

Paraffins formation as secondary reaction:

$$nCO + (2n+1)H_2 \leftrightarrow C_nH_{2n+2} + nH_2O \quad (n=1\text{-}3) \qquad (5)$$

Carrying out these reactions in situ in the same reactor over a bifunctional catalyst displaces the thermodynamic equilibrium in Eqs. 1 and 2 as a consequence of the dehydration of the formed methanol (Eq. 3). Consequently, lower pressure is required and it is possible to operate at higher temperature than in the synthesis of methanol, what leads to a higher reaction rate.[13-15] Due to these advantages, the prize estimated for the DME produced from synthesis gas via direct synthesis (syngas to DME or STD process) is lower than the diesel price in the current U.S. market.[16]

Besides, the incorporation of CO_2 as a reactant, co-fed together with syngas, is thermodynamically more feasible in the direct synthesis of DME than in the synthesis of

methanol.[14,17,18] Therefore, this process is considered to be a priority process among the routes for carbon capture and utilization (CCU), due to its capability to contribute for mitigating climate change.[19] Deepening in the environmental interest of the process, it is to note that the direct synthesis of DME requires a lower H_2/CO ratio than the synthesis of methanol, which is interesting for valorizing the syngas produced from biomass.[17,20,21] However, the availability of natural gas has boosted its interest as syngas source.[22,23]

The viability of the process is conditioned by the energy and environmental requirements. The economy, energy and exergy efficiency and CO_2 emissions depend on the source of syngas, CO_2 capture and reaction technologies, and especially on the availability of cheap renewable energy.[1] Kabir et al.[24] estimate in 32% the energy efficiency of the direct synthesis of DME from syngas generated by coal gasification, considering a CO_2 separation stage from syngas, with a net CO_2 emission of 2.91 kg/kg of DME. Nakyai and Saebea[25] compare the generation of syngas from natural gas, coal and biomass for the synthesis of DME in one and two stages, determining that the lower CO_2 emission (2-83 kJ/kg of syngas) corresponds to the steam gasification of biomass, even if the highest energy and exergy efficiency correspond to coal gasification. DinAli and Dincer[26] evaluate an overall energy and exergy efficiency of 28.75% and 32.54%, respectively, using CO_2 as raw material and using solar energy exclusively. These high efficiencies reach 50.2% and 45.0%, respectively producing syngas from CO_2/H_2O by means of chemical looping.[27] The exergy efficiency of the biomass gasification stage (key for the viability of this route) is increased by 15% through CO_2 enhanced gasification.[28] To meet the energy requirements of biomass gasification and DME synthesis Salman et al.[29] propose their integration with the existing combined heat and power plants.

Bearing the mentioned advantages and the environmental target of CO_2 utilization in mind, a great effort has been addressed toward upgrading the performance of the direct DME synthesis process. In the literature, many works deal with optimizing the operating conditions, and with the design, synthesis and tailoring of the properties of the catalysts used in the process.[4] The catalysts are composed of a metallic function, active for CO and CO_2 hydrogenation to methanol (Eqs.1-2), and for the r-WGS reaction (Eq. 4); and of an acid function, responsible for methanol dehydration to DME (Eq. 3). This latter function of the catalyst (acid function) needs to be of limited acid strength as to avoid the formation of hydrocarbons from methanol and DME through the hydrocarbon pool mechanism (Eq. 5).[30-32] Different zeotypes, such as HZSM-5, FER or MFI zeolites, ferrierite or SAPOs (SAPO-18, SAPO-11), of limited acid strength and density of the sites, give way to higher selectivity and stability than the γ–Al_2O_3 conventionally used for methanol dehydration to DME, due to their hydrophobic nature, the more suitable topology and the feasibility for tailoring the acidity.[3,31,33-37] As metallic functions, Cu-ZnO based catalysts are widely used.[38] Cu^0 and Cu^+ are considered to be the active species for methanol formation, while ZnO to be responsible for enhancing the dispersion of the active metal. Various promoters have been added to the aforementioned metallic function for increasing the stability of the active sites, and for the new scenario in which CO_2 is co-fed with syngas, the conventionally used Al_2O_3 promoter (traditionally used in the catalysts for methanol synthesis) has been replaced totally o partially by other metallic oxides (MnO, ZrO_2, Li_2O) to increase the selectivity and stability of the Cu-ZnO.[13,15,37,39-44] The configuration of the bifunctional catalyst (pelletizing of the individual functions separately or of their mixture and core-shell structure) has also been

studied, determining that for enhancing the stability of the metallic and acid functions and avoid their irreversible deactivation the direct contact between both functions must be limited as to avoid the migration of Cu, Al and Si ions between them.[45-48]

The hydrogenation of CO_2 and the incorporation of CO_2 as a reactant together with syngas, gives way to a large concentration of H_2O in the reaction medium through the r-WGS reaction (Eq. 4), hindering the formation of DME, due to the displacement of the methanol to DME dehydration reaction (Eq. 3) and the competitive adsorption in the active sites reducing the capacity of the metallic sites for methanol formation[49] and that of the acid sites for its dehydration.[50,51] As a consequence, the per pass conversion in the STD process is limited, and strategies for process intensification are required. Industrially, this situation is overcome in the synthesis of methanol by recycling the CO, CO_2 and H_2 stream. On the other hand, the background on hydrophilic membrane reactors for the synthesis of DME in the literature consists mainly of simulation studies.[52-54] Diban et al.[53,55] emphasize the interest of developing zeolite membranes capable for working under the operating conditions required in this process, that is, temperature above 250 ºC and high H_2O content in the medium. The use of membranes for removing H_2O from the medium has also been studied in other processes, such as Fischer-Tropsch synthesis[56,57], and is more viable than other strategies[58] to be installed in large-scale fixed-bed reactors. Bearing in mind the relevance of temperature for the permeation of H_2O, by means of permeation tests, Gorbe et al. propose zeolite A membrane as a feasible option for methanol synthesis.[59] The synergy of the reaction and the separation in the same unit, its simplicity and the possibility of automation and control, are attractive to improve the performance of the catalytic processes.[60]

In this work the following two strategies have been studied: i) recycling of the non-converted reactants; and ii) removing H_2O from the reaction medium as it is formed, using a H_2O permeable membrane. The influence of both strategies on the production of DME and on the conversion of CO_2 has been assessed. Usually the attention in the literature focuses on the selective production of DME, whereas this work focuses primarily on the conversion of CO_2 and on the effect of the reaction conditions on this conversion (in particular that of the CO_2/CO_x ratio in the feed). In this regard, it is to note that CO_2 is a byproduct in the DME synthesis process, and therefore, not only achieving its net conversion, but also limiting its generation is of great relevance for the sustainability of the process. Besides, it should be noted that the pursued scopes of maximizing DME production and CO_2 valorization correspond to opposite operating conditions,[51,61,62] and so, the relationship between these two targets is essential to combine both objectives. It is also interesting to assess the interest of the studied strategies considering catalyst deactivation.

2. METHODOLOGY

2.1. Catalyst and membrane

A bifunctional catalyst (CZMn/S) prepared by physical mixture of a CuO-ZnO-MnO metallic function and SAPO-18 as acid function has been used. The selection is based on its suitable catalytic activity for the conversion of CO_2, DME selectivity and regenerability.[37,61,63] The preparation conditions, composition, and its properties have been previously reported in these papers.

For studying the use of membranes for H_2O removal, the selectivity and permeability values have been selected according to the literature, focusing on the values considered to be adequate for temperatures above 200ºC and high pressure.[53,57]

Hence, 1.5 has been established as minimum value for H_2O/H_2 selectivity, and a permeability of $1 \cdot 10^{-7}$ mol $s^{-1}Pa^{-1}m^{-2}$ as optimal. According to the analysis carried out by Diban et al. these properties can be achieved with a H-SOD type zeolite[53], in which the permeation of oxygenated compounds (methanol and DME) is remarkably limited, which is a key feature for the selection of the membrane.[53,56,57,64-67]

2.2. Kinetic model

The kinetic model was previously established by our group for the CZMn/S bifunctional catalyst[62] (See Supporting Information). The model comprises the kinetic equations (Eqs. S1-S5) of the individual reactions involved in the reaction scheme (Eqs. 1-5) along with the deactivation kinetics (Eq. S9). This allows predicting the yielding products and the evolution with time on stream of the concentration of the components of the reaction medium in a wide range of operating conditions (250-350 ºC; 10 to 40 bar; space time between 1.25 and 20 $g_{cat}h(mol_C)^{-1}$; H_2/CO_x ratios in the feed, 3-4; and CO_2/CO_x ratios in the feed from 0 to 1.

2.3. Simulation of the Reactors

Using the kinetics previously reported for the simulation of the packed-bed reactor (PBR) with recirculation, a simulation program has been developed for assessing the influence of the operating conditions on the studied indices. The program developed in MATLAB

requires the following starting data: temperature, pressure, CO_2/CO_x and H_2/CO_x ratios in the feed, and time on stream and space time vectors. Subsequently, it integrates the differential equation system to calculate the product stream composition and the activity of the catalyst in the studied conditions.

In the packed-bed membrane reactor (PBMR) resolution program, additionally to the starting values defined previously (thus, operating conditions and kinetic parameters), data regarding the H_2O permeability of the membrane, permeance selectivity between H_2O and other components in the reaction medium, catalyst dilution and information on the configuration of the permeate section are also required. This program solves the mass conservation equations (global and individual for each component) for a differential volume of the reactor (considering plug-flow) in both the reaction and the permeate sections (Figure 1). Thus:

- In the reaction section:

$$\frac{d(F_r X_i)}{dz} = \rho \quad (\pi/4) d_r^2 r_i - Pm_i \pi d_m \Delta P_i = X_i \frac{d(F_r)}{dz} + F_r \frac{d(X_i)}{dz} \qquad (6)$$

where, d_m and d_r are the diameters of the membrane and the catalytic reactor, respectively; F_r is the molar flowrate in equivalent carbon units, $mol_C\ s^{-1}$, $mol_i\ Pa^{-1}\ s^{-1}\ m^{-2}$; r_i the formation rate of component i, $mol_i\ (g_{cat})^{-1}\ s^{-1}$; X_i the molar fraction of each component i; z the longitudinal position, m; ΔP_i the partial pressure difference of each component i between the reaction and the permeate sections.

The permeability of component i through the membrane is:

$$Pm_i = \frac{Pm_{H_2O}}{S_{H_2O/i}} \quad (7)$$

being $S_{H2O/i}$ the permeation selectivity of H_2O over component i; and $\Delta P_i = (P_{ri} - P_{Pi})$ (8)

where P_{ri}, is the partial pressure of each component i in the reaction section and; P_{Pi}, that in the permeate section. These terms are related to the total pressure as follows:

$$P_{ri} = P \frac{X_i/n_i}{\sum X_i/n_i} \quad (9)$$

$$P_{Pi} = P y_{Pi} \quad (10)$$

where, n_i is the number of C atoms in component i.

- In the permeate section:

$$\frac{d(F_P y_{Pi})}{dz} = Pm_i \pi d_m \Delta P_i = y_{Pi} \frac{d(F_P)}{dz} + F_P \frac{d(y_{Pi})}{dz} \quad (11)$$

where, F_P is he molar flowrate in the permeate section, in mol s^{-1}; and y_{Pi} the molar fraction of each component i in the same section.

In the abovementioned mass balances, the evolution of the flowrates with the longitudinal position in the reactor is determined as follows:

$$-\frac{dF_r}{dz} = \sum^{N^o \text{ organic compounds}} Pm_i \pi d_m \Delta P_i \quad (12)$$

$$\frac{dF_P}{dz} = \sum^{N^o \text{compounds}} Pm_i \pi d_m \Delta P_i \quad (13)$$

In order to solve the mass balances for each component i (Eqs. 6 and 11), they have been referred to the space time ($\tau=W/F_0$). As the resulting equations must be solved together with the mass balance in each of the sections (reaction and permeate), the equations to be solved are:

- In the reaction section:

Global balance:
$$\frac{d(F_r/F_0)}{d\tau} = \lambda \sum_{1}^{N^o\,organic\;compounds} n_i Pm_i \Delta P_i \qquad (14)$$

Individual balance:
$$\frac{dX_i}{d\tau} = (F_0/F_r)\left(r_i - X_i \frac{d(F_r/F_0)}{d\tau} - \lambda Pm_i \Delta P_i \right) \qquad (15)$$

In these equations, term λ quantifies the area of membrane per solid mass unit (catalyst + inert) in the catalytic bed as defined in Eq. 16:

$$\lambda = \frac{\pi d_m}{(\pi/4) d_r^2 \rho} \qquad (16)$$

- In the permeate section:

Global balance:
$$\frac{d(F_P/F_0)}{d\tau} = \lambda \sum Pm_i \Delta P_i \qquad (17)$$

Individual balance:
$$\frac{dy_{Pi}}{d\tau} = \frac{F_0 \lambda Pm_i \Delta P}{F_P} - y_{Pi} \frac{d(F_P/F_0)}{d\tau} \qquad (18)$$

3. RESULTS AND DISCUSSION

3.1. Recirculation

With this strategy, a fraction of the gases in the product stream (H_2, CO, CO_2 and hydrocarbons) is recycled, which has previously been separated from the oxygenated products (H_2O, DME and MeOH) by condensation (Figure 2). The fraction of recycled gas has been quantified as:

$$\varphi = \frac{G_R}{G_{NR}} \tag{19}$$

where G_R and G_{NR} are the flowrates of the recycled gas and that exiting the system, respectively.

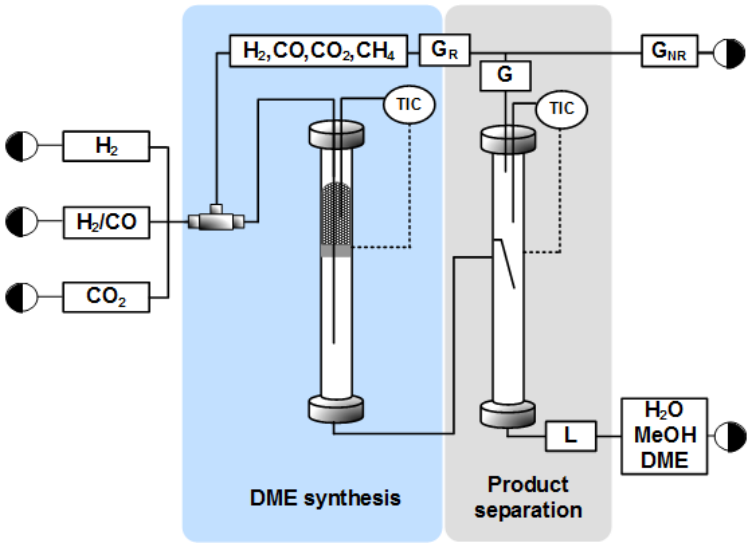

Figure 1. Diagram of the gas stream recirculation.

As for assessing the results, CO_2 conversion (X_{CO_2}) has been defined as the converted fraction of CO_2 (Eq. 20), and DME yield (Y_{DME}, Eq. 21) as the ratio between the molar flowrate of the produced DME (in carbon units) and the molar flowrate of CO_x in the feed.

$$X_{CO_2} = \frac{F^0_{CO_2} - F_{CO_2}}{F^0_{CO_2}} 100 \quad (20)$$

$$Y_{DME} = \frac{n_{DME} \cdot F_{DME}}{F^0_{COx}} 100 \quad (21)$$

where, $F^0_{CO_2}$ and F^0_{COx} are the molar flow rates of CO_2 and CO_x in the feed stream, respectively; while F_{CO_2} and F_{DME} are the molar flow rates of CO_2 and DME in the product stream, respectively; being n_{DME} the number of C atoms in DME.

It should be noted that with the definition of CO_2 conversion in Eq. 20, the positive value corresponds to its effective valorization into oxygenates (methanol and DME) or CO, while negative values indicate that there is CO_2 formation in the process, due to the importance of the WGS reaction (reverse of Eq. 4).

Figure 2 shows the curves of similar CO_2 conversion (graph a) and similar DME yield (graph b), for different values of space time and recirculation factor. These results provided as an example correspond to the following reaction conditions: 275 ºC, 30 bar, CO_2/CO_x = 0.25, H_2/CO_x = 3, 5 h time on stream.

CO_2 conversion (Figure 2a) increases with diminishing space time, and, to a major extent, when the recirculation of the non-converted reactants increases. For φ values above 0.8 the effect of space time is barely relevant, and CO_2 conversion surpasses the 70 %. Similarly, as to the DME yield concerns, the favorable effect of recirculation is greater than that of increasing space time (Figure 2b). Thus, DME yield exceeds 30 % for φ values above 0.8 with space time values over 5 $g_{cat}h(mol_C)^{-1}$. For higher φ values DME yield improves regardless of space time.

Comparing the values obtained with those obtained without recirculation, that is, the values corresponding to φ= 0 in the figure, it is noteworthy that the recirculation of the non-converted reactants contributes favorably to improving both CO_2 conversion and DME yield. For the conditions plotted in Figure 2 (CO_2/CO_x= 0.25), and a recirculation factor of φ= 0.85, not only the process stops producing CO_2 (for 5 $g_{cat}h(mol_C)^{-1}$ X_{CO2}= -10% without recirculation), but its conversion exceeds a positive value of 10 %, achieving therefore its net valorization. As to DME regards, with this same recirculation factor the obtained yield value more than triples that obtained without recirculation, boosting from 10 % to 35 %.

As a consequence of catalyst deactivation, these values vary with time on stream. However, the recirculation of a fraction of the non-converted reactants mitigates the effect of the deactivation on the conversion of CO_2 (Figure 3) since the composition in the medium is modified. In this manner, for φ values over 0.8, CO_2 conversion is almost constant with time on stream (Figure 3a), whereas DME yield decays, even if it is less significant for high recirculation values (Figure 3b).

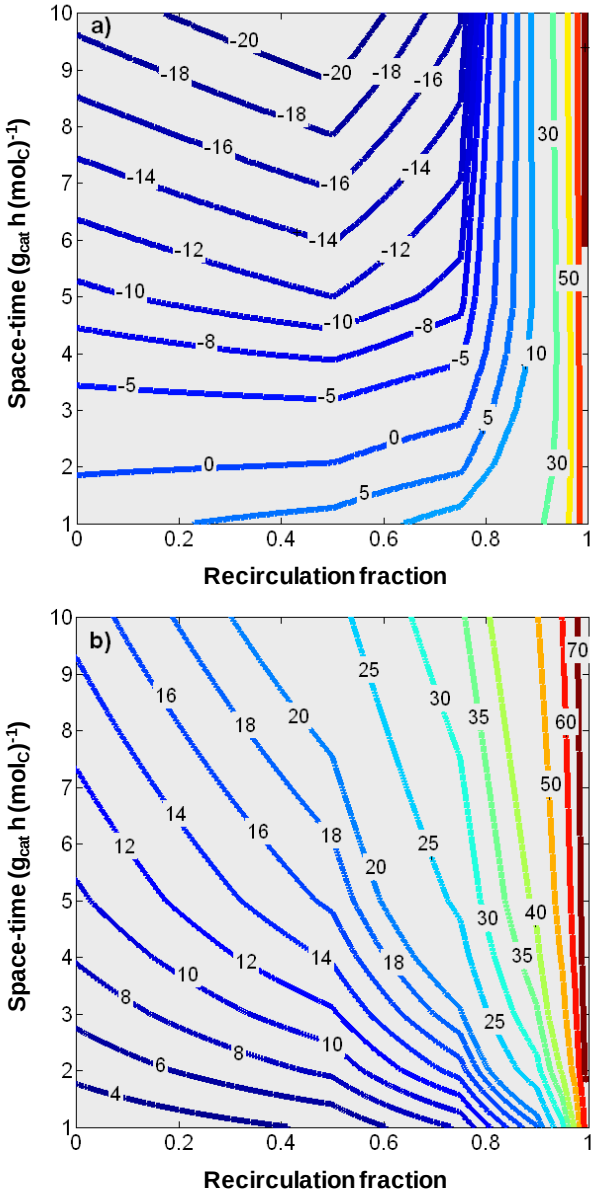

Figure 2. Contour maps of CO_2 conversion (a) and DME yield (b) for different values of space time and recirculation factor. Reaction conditions: 275 ºC; 30 bar; time on stream, 5 h; H_2+CO+CO_2 feed, CO_2/CO_x, 0.25; H_2/CO_x, 3.

The results depicted in Figure 4 correspond to a CO_2/CO_x ratio of 0.50 in the feed, and compared to those corresponding to CO_2/CO_x = 0.25 (Figure 3), show that increasing the CO_2/CO_x ratio in the feed increases the CO_2 valorization capacity and decreases the

yield of DME, in agreement with that reported by other authors.[15,68] This difference is attenuated by increasing the recirculation factor and for a value around 0.97, a CO_2 conversion value of 70 % and a DME yield of 60 % are obtained, regardless of the CO_2/CO_x ratio.

Attending to the data in Figure 4, it is concluded that the intensification of the process (improvement of the studied indices) is greater the greater the concentration of CO_2 in the feed. Nevertheless, it is to note that the increase in DME yield is very significant, at any recirculation rate, regardless of the fed CO_2/CO_x ratio. As an example, even if DME yield at 10 h of time on stream is a 50 % higher when feeding CO_2/CO_x= 0.25 (Figure 3) than feeding CO_2/CO_x= 0.50 (Figure 4), at high recirculation factor values the difference is mitigated, reaching values of 40 % and 35 %, respectively for φ = 0.9.

These results highlight the great applicability of the recirculation strategy, and the convenience of recirculating the largest fraction of non-converted reactants possible. This is a simple strategy to implement that gives rise to very promising results from the CO_2 valorization perspective.

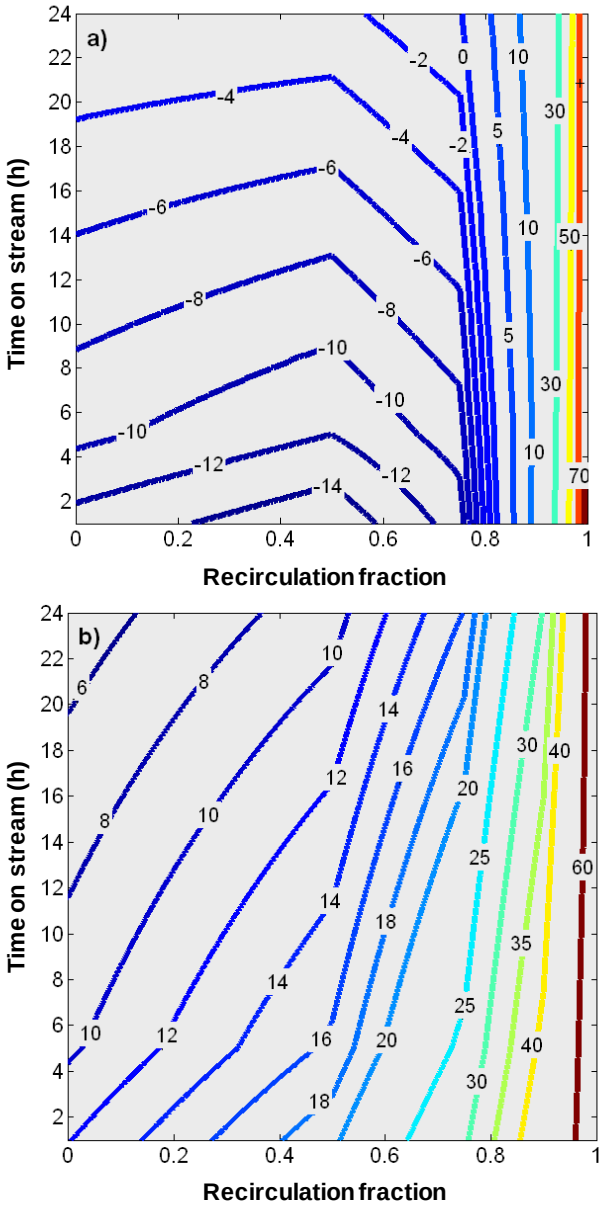

Figure 3. Contour maps of CO_2 conversion (a) and DME yield (b) for different values of time on stream and recirculation factor. Reaction conditions: 275 ºC; 30 bar; space time, 5 $g_{cat}h(mol_C)^{-1}$; H_2+CO+CO_2 feed, CO_2/CO_x, 0.25; H_2/CO_x, 3.

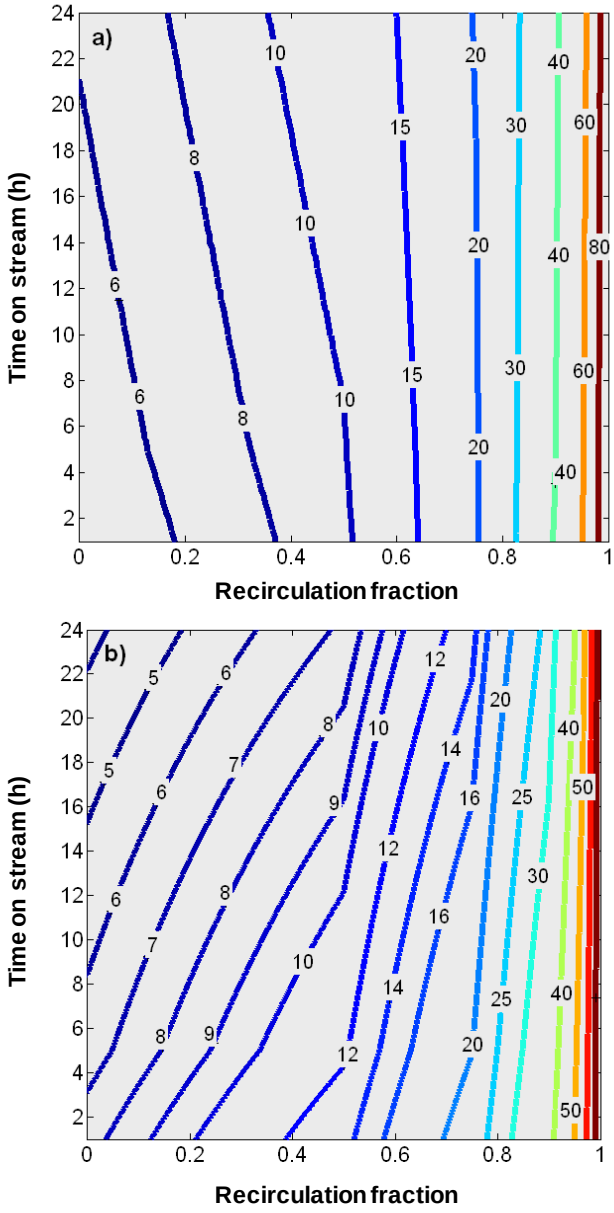

Figure 4. Contour maps of CO_2 conversion (a) and DME yield (b) for different values of time on stream and recirculation factor. Reaction conditions: 275 ºC; 30 bar; space time, 5 $g_{cat}h(mol_C)^{-1}$; H_2+CO+CO_2 feed, CO_2/CO_x, 0.5; H_2/CO_x, 3.

3.2. Packed-Bed Membrane Reactor

In this section the feasibility of implementing a membrane into the conventionally used packed-bed reactors has been studied. This configuration, described in Figure 5, pursues separating part of the H_2O generated in the reaction section by its permeation through the membrane and its subsequent sweeping in the permeate section. The driving force is given by the difference in molar fraction between the reaction and permeate sections. Thus, the maximum ΔP between the reactor outlet and the permeate outlet streams has been settled below 10 cm H_2O column, which is lower than the 1 % of the total pressure used in the process. The effect of certain properties of the membrane (water permeability, permeation selectivity between H_2O and other components, catalyst dilution level and the sweeping mode) on the reaction indices has been studied. As sweeping strategies different options have been evaluated, thus, flowing mode in co- or counter-current; and the use of H_2 or H_2+CO+CO_2 mixtures as sweeping agents. Additionally, the results derived from the simulations have been compared with those experimentally obtained in a packed-bed reactor.

Using the simulation program described in Section 2.3, the effect of the two most relevant properties of the membrane (H_2O permeability and permeation selectivity of H_2O over H_2) on the conversion of the fed CO_2 and on the production of DME have been assessed, considering H_2O the only permeating compound. These properties condition the ratio between the flowrates of permeate H_2O/generated H_2O. For our goal, a moderate H_2O permeance is enough, while the relevance of the H_2O/H_2 permeance selectivity is to be highlighted (Figure S1). Coinciding with Diban et al.[53] a H_2O

permeation of $1 \cdot 10^{-7}$ mol $s^{-1}Pa^{-1}m^{-2}$ has been established as most suitable, as the permeated H_2O/generated H_2O ratio goes through a maximum in this value. Likewise, 1.5 has been established as the minimum H_2O to H_2 selectivity.

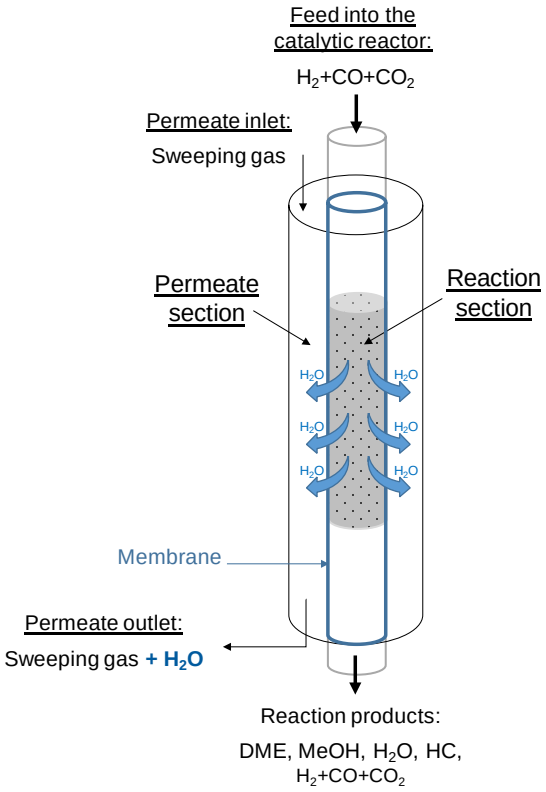

Figure 5. Diagram of the packed-bed membrane reactor.

Figure 6 displays for different values of H_2O/H_2 selectivity vs H_2O permeability the maps of CO_2 conversion (graph a) and DME yield (graph b) values obtained using H_2 as sweeping gas in the permeate section (in the same flow rate as the total flowrate fed into the reaction section, that is 60 cm^3 min^{-1} and in the same direction, co-current mode) to sweep the permeating H_2O for the following reaction conditions: 275 ºC, 30 bar, 10.18 $g_{cat}h$ $(mol_C)^{-1}$, $H_2+CO+CO_2$ feed with CO_2/CO_x ratio of 1 and H_2/CO_x ratio of 3.

These conditions correspond to high CO_2 conversion values, favored by the use of a membrane.

As depicted in Figure 6a, it can be observed that for a low value of H_2O permeability (below $1 \cdot 10^{-7}$ mol s^{-1} m^{-2} Pa^{-1}) the conversion of CO_2 is not dependent on the H_2O/H_2 selectivity, and increases upon increasing H_2O permeability, while it is hampered by increasing H_2O/H_2 selectivity, even if this effect is progressively lower. On the other hand, increasing H_2O permeability enhances DME yield, whereas it is almost independent of H_2O/H_2 selectivity under the conditions studied.

To deepen in the study of the influence of using a membrane for producing DME and valorizing CO_2 in the STD process, the improvement obtained over working with conventional packed-bed reactors has been assessed, and different sweeping strategies have been tested. For this purpose, H_2O permeability has been settled in $1 \cdot 10^{-7}$ mol s^{-1} m^{-2} Pa^{-1} and the H_2O to H_2 permeance selectivity in 4. These values have been selected as they are theoretically within the possibilities of the membranes already used in the literature, among which, as previously stated, H-SOD (hydroxyl sodalite) provides H_2O permeance and H_2O/H_2 permeance selectivity values over those required in the present process, with limited permeance of other oxygenated compounds, as methanol and DME in this case.[55,57,64-66]

In Figure 7 it has been depicted the upgrade of CO_2 conversion (graph a) and DME yield (graph b) achievable using a membrane with the abovementioned properties, over the values of these two indices obtained experimentally in a conventional packed-bed reactor for different CO_2/CO_x ratios in the feed[61], using H_2 as sweeping agent as in Figure 6.

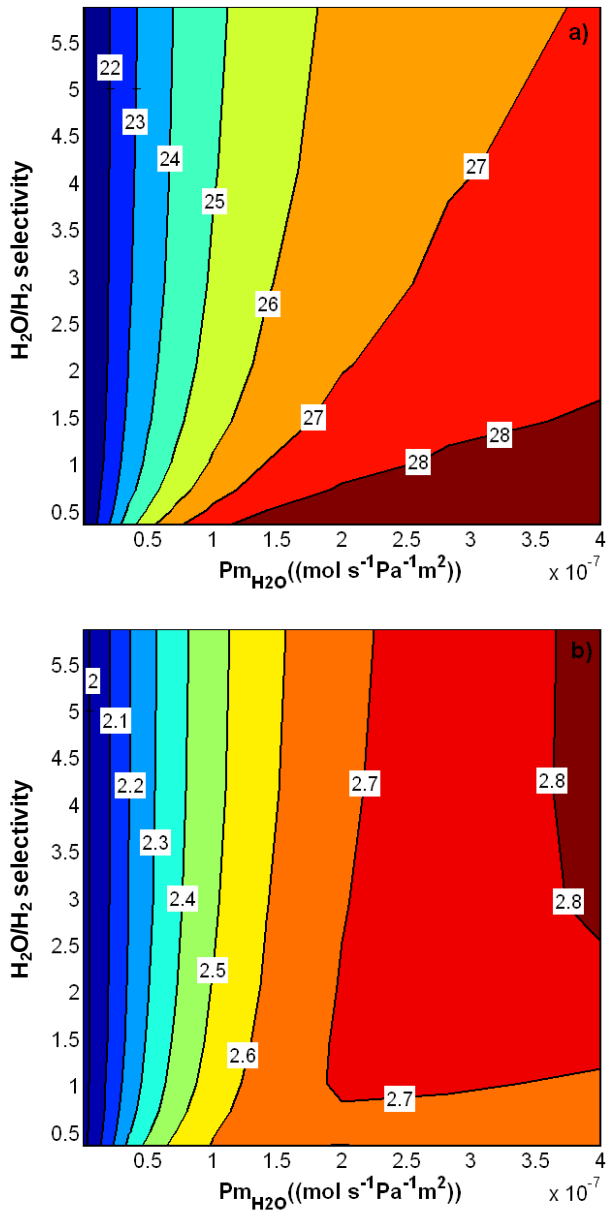

Figure 6. Contour maps of CO_2 conversion (a) and DME yield (b) for different values of the membrane properties, H_2O/H_2 selectivity and H_2O permeability. Reaction conditions: 275 ºC, 30 bar; 10.18 $g_{cat}h(mol_C)^{-1}$; H_2+CO+CO_2; CO_2/CO_x= 1; H_2/CO_x, 3. Permeate section: sweeping with H_2 in co-current mode.

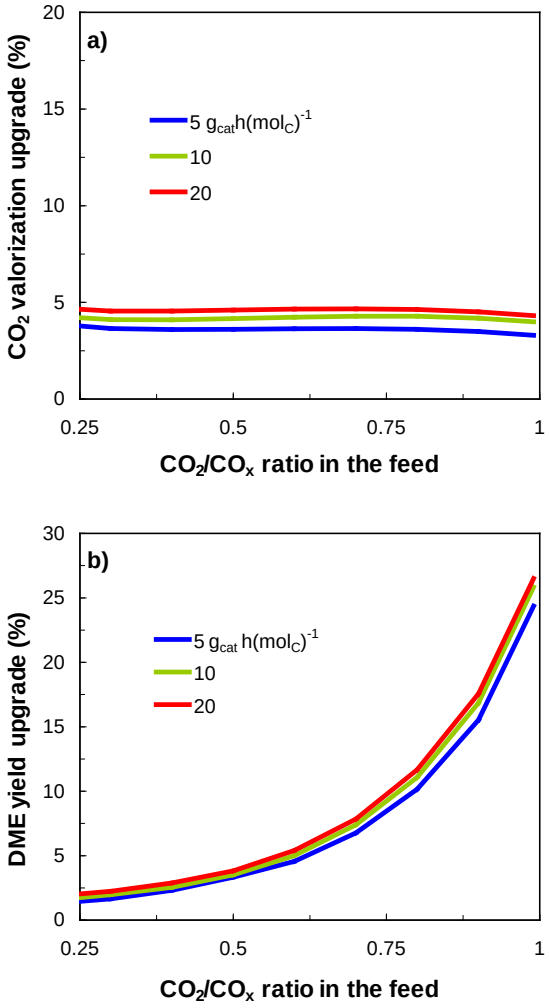

Figure 7. Effect of CO_2/CO_x ratio in the feed on the upgrade of CO_2 conversion (a) and DME yield (b) using a PBMR for different values of space time. Reaction conditions: 275 ºC, 30 bar; H_2+CO+CO_2 feed; H_2/CO_x, 3. Permeate section: sweeping with H_2 in co-current mode.

It can be observed that the upgrade in CO_2 conversion vaguely diminishes with increasing CO_2/CO_x ratio (Figure 7a). However, using the membrane CO_2 conversion increases in all cases a 3.5-4 % over the value obtained in a packed-bed reactor, and this advantage is slightly more relevant upon increasing space time.

The effect on DME yield is more relevant (Figure 7b). The gain of DME production when using a PBMR increases steeply upon increasing CO_2/CO_x ratio in the feed reaching a difference of a 25 % for pure H_2+CO_2 feeds, that is, for $CO_2/CO_x= 1$. As in the case of CO_2 conversion, the effect is more favorable the higher the space time, even if it is not very relevant.

Figure 8 comprises the effect of using a flowrate with the same composition as that fed to the reaction section ($H_2+CO+CO_2$) as sweeping gas instead of H_2. The curves plotted in this figure show narrow difference of the strategy of sweeping in co-current mode over the counter-current mode, trend also observed when using H_2 as sweeping agent.

The results in Figures 7 and 8 show non-relevant differences between the H_2 and $H_2+CO+CO_2$ sweeping agents in co-current mode.

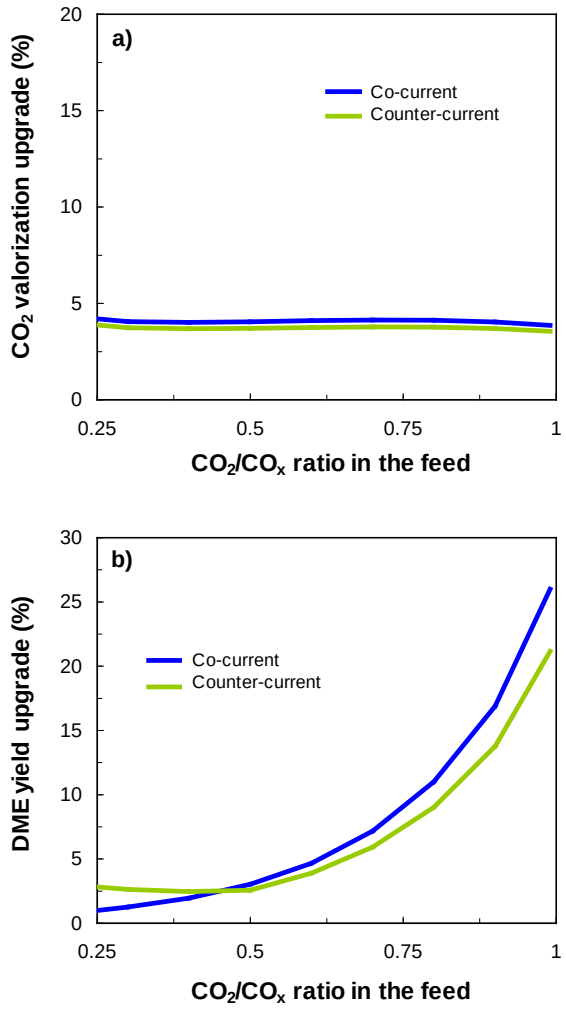

Figure 8. Comparison between the effect on CO_2 conversion (a) and DME yield upgrade (b) obtained with the strategies of sweeping in co-current and counter-current mode in a PBMR. Reaction conditions: 275 ºC, 30 bar; 20 $g_{cat}h\ (mol_C)^{-1}$; H_2+CO+CO_2; H_2/CO_x, 3. Permeate section: sweeping with H_2+CO+CO_2; H_2/CO_x, 3 in the same composition as that fed to the reactor.

According to the results, overall, little differences have been observed between the sweeping strategies. However, the improvement obtained using a PBMR is relevant in all cases, not only for boosting DME production, but for not penalizing CO_2 conversion, and even for enhancing its conversion. This encourages the perspective of continuing with the research of membrane reactors, both by simulation and experimentally, in parallel with the development of materials with properties that improve the benefits considered in the previous simulations, along with other intensification strategies, as for example temperature gradients in the permeation section for improving separation, as proposed by Gorbe et al.[59] attending to the favorable results obtained in permeation tests (without catalytic reaction).

It should be mentioned that the results reported in this work do not permit to distinguish clearly the contribution to the results of the two effects obtained when using a membrane, thus: i) removing H_2O from the reaction medium; ii) the modification of the longitudinal distribution of the reactants and in particular of H_2. These features will require further simulation studies considering different properties of the membrane.

4.CONCLUSIONS

The recirculation of the non-converted reactants present in the product stream resulted to be an effective strategy to combine the two pursued targets (high DME production and high CO_2 conversion). Besides, this strategy also helps to reduce catalyst deactivation. Thus, for a recirculation factor above 0.8, DME yield is independent of the space time used and the achieved CO_2 conversion remains almost constant with time on stream. Thus, with a CO_2/CO_x ratio of 0.25 in the feed and a high recirculation factor, of 0.97, at 275 ºC and 30 bar, using 5 $g_{cat}h\ (mol_C)^{-1}$, a CO_2 conversion of 70 % and a DME yield of 60 % is achieved.

Likewise, the implementation of a membrane into the conventional packed-bed reactor also gives way to promising results. However, the difficulty of obtaining suitable membranes capable for operating at the reaction conditions required in the STD process without suffering deterioration of its properties is still under study. Using in the simulations a membrane with a H_2O permeability of $1 \cdot 10^{-7}$ mol s^{-1} m^2 Pa^{-1} and a H_2O/H_2 selectivity of 4, values feasibly achievable according to the literature, the improvements obtained in the results are noteworthy. The use of a membrane with these properties (as the H-SOD zeolite) enhances the conversion of CO_2, improving between a 3.5 and a 5% over a PBR, almost independently of the CO_2/CO_x ratio fed into the reactor, and its effect is favored by the increase of space time. The favorable effect on the production of DME is significantly more noticeable, and the upgrade over the conventional packed-bed reactor increases exponentially upon increasing the CO_2/CO_x ratio (in the reactor feed), reaching an upgrade of a 25 % for pure CO_2 hydrogenation. To deepen in the study of the packed-bed membrane reactor different permeate sweeping strategies have been studied,

concluding that the sweeping mode, that is co-current (parallel to the flow through the reactor) and counter-current mode, or using H_2 or H_2+CO+CO_2 as sweeping agent does not give way to relevant differences.

SUPPORTING INFORMATION

Reaction scheme and kinetic parameters for the kinetic modeling of the direct DME synthesis using a CuO-ZnO-MnO/SAPO-18 bifunctional catalyst. Influence of membrane properties on the Permeate H_2O flowrate / generated H_2O flowrate.

This information is available free of charge via the internet at http://pubs.acs.org/

ACKNOWLEDGMENTS

This work has been carried out with the financial support of the Ministry of Economy and Competitiveness of the Spanish Government (CTQ2016-77812-R), the Basque Government (Project IT1218-19), the ERDF funds and the European Commission (HORIZON H2020-MSCA RISE-2018. Contract No. 823745).

NOMENCLATURE

ΔP_i Partial pressure difference of each component i between the reaction and the permeate sections, Pa.

φ Fraction of recycled gas, recirculation factor.

λ Area of membrane per solid mass unit.

ρ Density of the catalyst in the catalytic bed, $g \cdot cm^{-3}$.

τ Space time, $g_{cat}\ h\ (mol_C)^{-1}$.

CO_x $CO + CO_2$ mixture.

d_m, d_r diameters of the membrane and the catalytic reactor, respectively, mm.

F_0 Molar flowrate in the feed, $mol \cdot h^{-1}$.

F_i Molar flowrate of component i in the product stream, in equivalent C units, $mol_C \cdot h^{-1}$.

F_{COx}^0, F_{CO2}^0 Molar flowrate of $CO+CO_2$ mixture, or of CO_2, respectively, in the reactor feed stream, in equivalent C units, $mol_C \cdot h^{-1}$.

F_r Molar flowrate in the reaction section, $mol \cdot h^{-1}$.

F_p Molar flowrate in the permeate section, $mol \cdot h^{-1}$.

G_R Flowrate of recycled gas, $mol \cdot h^{-1}$.

G_{NR} Flowrate of not-recycled gas, thus, exiting the system, $mol \cdot h^{-1}$.

n_i	Number of carbon atoms in component i.
Pm_i	Permeability of component i through the membrane, $mol_i\ Pa^{-1}\ s^{-1}\ m^{-2}$.
P_{ri}, P_{pi}	Partial pressure of component i in the reaction and permeate sections, respectively, Pa.
r_i	Formation rate of component i, $mol_i\ (g_{cat} \cdot h)^{-1}$.
$S_{H2O/i}$	Permeance selectivity between H_2O and component i.
W	Catalyst mass, g.
X_{CO_2}	CO_2 conversion, %.
X_i	Molar fraction of each component i.
Y_{DME}	DME yield, %.
y_i	Molar fraction of component i.
z	longitudinal position, m.

REFERENCES

(1) Michailos, S.; McCord, S.; Sick, V.; Stokes, G.; Styring, P. Dimethyl Ether Synthesis via Captured CO_2 Hydrogenation within the Power to Liquids Concept: A Techno-Economic Assessment. *Energy Convers. Manag.* **2019**, *184*, 262–276.

(2) Leonzio, G. State of Art and Perspectives about the Production of Methanol, Dimethyl Ether and Syngas by Carbon Dioxide Hydrogenation. *J. CO2 Util.* **2018**, *27*, 326–354.

(3) Azizi, Z.; Rezaeimanesh, M.; Tohidian, T.; Rahimpour, M. R. Dimethyl Ether: A Review of Technologies and Production Challenges. *Chem. Eng. Process. Process Intensif.* **2014**, *82*, 150–172.

(4) Mondal, U.; Yadav, G. D. Perspective of Dimethyl Ether as Fuel: Part I. Catalysis. *J. CO2 Util.* **2019,** *32*, 299-320.

(5) Semelsberger, T. A.; Borup, R. L.; Greene, H. L. Dimethyl Ether (DME) as an Alternative Fuel. *J. Power Sources* **2006**, *156* (2), 497–511.

(6) Arcoumanis, C.; Bae, C.; Crookes, R.; Kinoshita, E. The Potential of Di-Methyl Ether (DME) as an Alternative Fuel for Compression-Ignition Engines: A Review. *Fuel* **2008**, *87* (7), 1014–1030.

(7) Kim, M. Y.; Yoon, S. H.; Ryu, B. W.; Lee, C. S. Combustion and Emission Characteristics of DME as an Alternative Fuel for Compression Ignition Engines with a High Pressure Injection System. *Fuel* **2008**, *87* (12), 2779–2786.

(8) Wen, Z.; Li, Z.; Ge, Q.; Zhou, Y.; Sun, J.; Abroshan, H.; Li, G. Robust Nickel

Cluster@Mes-HZSM-5 Composite Nanostructure with Enhanced Catalytic Activity in the DTG Reaction. *J. Catal.* **2018**, *363*, 26–33.

(9) Pérez-Uriarte, P.; Ateka, A.; Gamero, M.; Aguayo, A. T.; Bilbao, J. Effect of the Operating Conditions in the Transformation of DME to Olefins over a HZSM-5 Zeolite Catalyst. *Ind. Eng. Chem. Res.* **2016**, *55* (23), 6569-6578.

(10) Al-Dughaither, A. S.; de Lasa, H. Neat Dimethyl Ether Conversion to Olefins (DTO) over HZSM-5: Effect of SiO_2/Al_2O_3 on Porosity, Surface Chemistry, and Reactivity. *Fuel* **2014**, *138*, 52–64.

(11) Oar-Arteta, L.; Remiro, A.; Aguayo, A. T.; Olazar, M.; Bilbao, J.; Gayubo, A. G. Development of a Bifunctional Catalyst for Dimethyl Ether Steam Reforming with $CuFe_2O_4$ Spinel as the Metallic Function. *J. Ind. Eng. Chem.* **2016**, *36*, 169–179.

(12) Faungnawakij, K.; Shimoda, N.; Viriya-empikul, N.; Kikuchi, R.; Eguchi, K. Limiting Mechanisms in Catalytic Steam Reforming of Dimethyl Ether. *Appl. Catal. B Environ.* **2010**, *97* (1–2), 21–27.

(13) De Falco, M.; Capocelli, M.; Centi, G. Dimethyl Ether Production from CO_2 Rich Feedstocks in a One-Step Process: Thermodynamic Evaluation and Reactor Simulation. *Chem. Eng. J.* **2016**, *294*, 400–409.

(14) Ateka, A.; Pérez-Uriarte, P.; Gamero, M.; Ereña, J.; Aguayo, A. T.; Bilbao, J. A Comparative Thermodynamic Study on the CO_2 Conversion in the Synthesis of Methanol and of DME. *Energy* **2017**, *120*, 796-804.

(15) Chen, W.-H.; Lin, B.-J.; Lee, H.-M.; Huang, M.-H. One-Step Synthesis of Dimethyl Ether from the Gas Mixture Containing CO_2 with High Space Velocity. *Appl. Energy* **2012**, *98*, 92–101.

(16) Mevawala, C.; Jiang, Y.; Bhattacharyya, D. Techno-Economic Optimization of Shale Gas to Dimethyl Ether Production Processes via Direct and Indirect Synthesis Routes. *Appl. Energy* **2019**, *238*, 119–134.

(17) Stangeland, K.; Li, H.; Yu, Z. Thermodynamic Analysis of Chemical and Phase Equilibria in CO_2 Hydrogenation to Methanol, Dimethyl Ether, and Higher Alcohols. *Ind. Eng. Chem. Res.* **2018**, *57* (11), 4081–4094.

(18) Suwannapichat, Y.; Numpilai, T.; Chanlek, N.; Faungnawakij, K.; Chareonpanich, M.; Limtrakul, J.; Witoon, T. Direct Synthesis of Dimethyl Ether from CO_2 Hydrogenation over Novel Hybrid Catalysts Containing a Cu–ZnO–ZrO_2 Catalyst Admixed with WO_x/Al_2O_3 Catalysts: Effects of Pore Size of Al_2O_3 Support and W Loading Content. *Energy Convers. Manag.* **2018**, *159*, 20–29.

(19) Fernández-Dacosta, C.; Stojcheva, V.; Ramirez, A. Closing Carbon Cycles: Evaluating the Performance of Multi-Product CO_2 Utilisation and Storage Configurations in a Refinery. *J. CO2 Util.* **2018**, *23*, 128–142.

(20) Catizzone, E.; Bonura, G.; Migliori, M.; Frusteri, F.; Giordano, G. CO_2 Recycling to Dimethyl Ether: State-of-the-Art and Perspectives. *Molecules* **2018**, *23* (1), 31-59.

(21) Olah, G. A.; Goeppert, A.; Prakash, G. K. S. Chemical Recycling of Carbon

Dioxide to Methanol and Dimethyl Ether: From Greenhouse Gas to Renewable, Environmentally Carbon Neutral Fuels and Synthetic Hydrocarbons. *J. Org. Chem.* **2009**, *74* (2), 487–498.

(22) Lerner, A.; Brear, M. J.; Lacey, J. S.; Gordon, R. L.; Webley, P. A. Life cycle analysis (LCA) of low emission methanol and di-methyl ether (DME) derived from natural gas. *Fuel*. **2018**, *220*, 871-878.

(23) Farsi, M.; Freki Lari, M.; Rahimpour, M. R. Development of a green process for DME production based on the methane tri-reforming. J. Taiwan Inst. Chem. Eng. *In press*. https://doi.org/10.1016/j.jtice.2019.10.001

(24) Kabir, K. B.; Hein, K.; Battacharya, S. Process modelling of dimethyl ether production from Victorian brown coal—Integrating coal drying, gasification and synthesis processes.*Comp. Chem. Eng.* **2013**, *48*, 96-104.

(25) Nakyai, T.; Saebea, D. Exergoeconomic comparison of syngas production from biomass, coal, and natural gas for dimethyl ether synthesis in single-step and two-step processes. *J. Cleaner. Production*. **2019**, *241*, 118334.

(26) DinAli, M.; Dincer, I. Performance assessment of a new solar energy based cogeneration system for dimethyl-ether and electricity production. *Solar Energy*. **2019**, *190*, 337-349.

(27) Farooqui, A.; Di Tomaso, F.; Bose, A.; Ferrero, D.; Llorea, J.; Santarelli, M. Techno-economic and exergy analysis of polygeneration plant for power and DME production with the integration of chemical looping CO_2/H_2O splitting. *Energy*

Conver. Manage. **2019**, *186*, 200-219.

(28) Parvez, A. M.; Wu, T.; Li, S.; Miles, N.; Mujtaba, I. M. Bio-DME production based on conventional and CO_2-enhanced gasification of biomass: A comparative study on exergy and environmental impacts. *Biomass Bioenergy*. **2018**, *110*, 105-113.

(29) Salman, C. A.; Naqvi, M.; Thorin, E.; Yan, J. Gasification Process Integration with Existing Combined Heat and Power Plants for Polygeneration of Dimethyl Ether or Methanol: A Detailed Profitability Analysis. *Appl. Energy* **2018**, *226*, 116–128.

(30) Bjørgen, M.; Svelle, S.; Joensen, F.; Nerlov, J.; Kolboe, S.; Bonino, F.; Palumbo, L.; Bordiga, S.; Olsbye, U. Conversion of Methanol to Hydrocarbons over Zeolite H-ZSM-5: On the Origin of the Olefinic Species. *J. Catal.* **2007**, *249* (2), 195–207.

(31) Sánchez-Contador, M.; Ateka, A.; Aguayo, A. T.; Bilbao, J. Behavior of SAPO-11 as Acid Function in the Direct Synthesis of Dimethyl Ether from Syngas and CO_2. *J. Ind. Eng. Chem.* **2018**, *63*, 245–254.

(32) Ilias, S.; Bhan, A. Mechanism of the Catalytic Conversion of Methanol to Hydrocarbons. *ACS Catal.* **2013**, *3* (1), 18–31.

(33) Sun, J.; Yang, G.; Yoneyama, Y.; Tsubaki, N. Catalysis Chemistry of Dimethyl Ether Synthesis. *ACS Catal.* **2014**, *4* (10), 3346–3356.

(34) An, X.; Zuo, Y. Z.; Zhang, Q.; Wang, D. Z.; Wang, J. F. Dimethyl Ether Synthesis from CO_2 Hydrogenation on a CuO-ZnO-Al_2O_3-ZrO_2/HZSM-5 Bifunctional

Catalyst. *Ind. Eng. Chem. Res.* **2008**, *47* (17), 6547–6554.

(35) Migliori, M.; Catizzone, E.; Aloise, A.; Bonura, G.; Gómez-Hortigüela, L.; Frusteri, L.; Cannilla, C.; Frusteri, F.; Giordano, G. New Insights about Coke Deposition in Methanol-to-DME Reaction over MOR-, MFI- and FER-Type Zeolites. *J. Ind. Eng. Chem.* **2018**, *68*, 196–208.

(36) Aguayo, A. T.; Ereña, J.; Sierra, I.; Olazar, M.; Bilbao, J. Deactivation and Regeneration of Hybrid Catalysts in the Single-Step Synthesis of Dimethyl Ether from Syngas and CO_2. *Catal. Today* **2005**, *106* (1–4), 265–270.

(37) Ateka, A.; Sierra, I.; Ereña, J.; Bilbao, J.; Aguayo, A. T. Performance of CuO–ZnO–ZrO_2 and CuO–ZnO–MnO as Metallic Functions and SAPO-18 as Acid Function of the Catalyst for the Synthesis of DME Co-feeding CO_2. *Fuel Process. Technol.* **2016**, *152*, 34–45.

(38) Ren, S.; Shoemaker, W. R.; Wang, X.; Shang, Z.; Klinghoffer, N.; Li, S.; Yu, M.; He, X.; White, T. A.; Liang, X. Highly Active and Selective Cu-ZnO Based Catalyst for Methanol and Dimethyl Ether Synthesis via CO_2 Hydrogenation. *Fuel* **2019**, *239*, 1125–1133.

(39) Bonura, G.; Cordaro, M.; Cannilla, C.; Mezzapica, A.; Spadaro, L.; Arena, F.; Frusteri, F. Catalytic Behaviour of a Bifunctional System for the One Step Synthesis of DME by CO_2 Hydrogenation. *Catal. Today* **2014**, *228*, 51–57.

(40) De Falco, M.; Capocelli, M. Chapter 5 – Direct Synthesis of Methanol and Dimethyl Ether From a CO_2-Rich Feedstock: Thermodynamic Analysis and

Selective Membrane Application. In *Methanol: Science and Engineering* (Part 1); Basile, A.; Dalena, F., Eds; Elsevier B.V., 2017; pp 113–128.

(41) Bonura, G.; Frusteri, F.; Cannilla, C.; Drago Ferrante, G.; Aloise, A.; Catizzone, E.; Migliori, M.; Giordano, G. Catalytic Features of CuZnZr–Zeolite Hybrid Systems for the Direct CO_2-to-DME Hydrogenation Reaction. *Catal. Today* **2016**, *277*, 48–54.

(42) Witoon, T.; Kidkhunthod, P.; Chareonpanich, M.; Limtrakul, J. Direct Synthesis of Dimethyl Ether from CO_2 and H_2 over Novel Bifunctional Catalysts Containing CuO-ZnO-ZrO_2 Catalyst Admixed with WO_x/ZrO_2 Catalysts. *Chem. Eng. J.* **2018**, *348*, 713–722.

(43) Zuo, H.; Mao, D.; Guo, X.; Yu, J. Highly Efficient Synthesis of Dimethyl Ether Directly from Biomass-Derived Gas over Li-Modified Cu-ZnO-Al_2O_3/HZSM-5 Hybrid Catalyst. *Renew. Energy* **2018**, *116*, 38–47.

(44) Koh, M. K.; Wong, Y. J.; Chai, S. P.; Mohamed, A. R. Carbon Dioxide Hydrogenation to Methanol over Multi-Functional Catalyst: Effects of Reactants Adsorption and Metal-Oxide(s) Interfacial Area. *J. Ind. Eng. Chem.* **2018**, *62*, 156–165.

(45) García-Trenco, A.; Martínez, A. A Rational Strategy for Preparing Cu–ZnO/H-ZSM-5 Hybrid Catalysts with Enhanced Stability during the One-Step Conversion of Syngas to Dimethyl Ether (DME). *Appl. Catal. A Gen.* **2015**, *493*, 40–49.

(46) Sánchez-Contador, M; Ateka, A.; Aguayo, A. T.; Bilbao, J. Direct synthesis of

dimethyl ether from CO and CO_2 over a core-shellstructured CuO-ZnO-ZrO_2@SAPO-11 catalyst. *Fuel Process. Technol.* **2018,** *179*, 258-268.

(47) Ateka, A.; Sánchez-Contador, M.; Ereña, J.; Aguayo, A. T.; Bilbao, J. Catalyst Configuration for the Direct Synthesis of Dimethyl Ether from CO and CO_2 Hydrogenation on CuO–ZnO–MnO/SAPO-18 Catalysts. *React. Kinet. Mech. Catal.* **2018**, *124* (1), 401-418.

(48) Ren, S.; Li, S.; Klinghoffer, N.; Yu, M.; Liang, X. Effects of Mixing Methods of Bifunctional Catalysts on Catalyst Stability of DME Synthesis via CO_2 Hydrogenation. *Carbon Resour. Convers.* **2019**, *2* (1), 85–94.

(49) Dadgar, F.; Myrstad, R.; Pfeifer, P.; Holmen, A.; Venvik, H. J. Direct Dimethyl Ether Synthesis from Synthesis Gas: The Influence of Methanol Dehydration on Methanol Synthesis Reaction. *Catal. Today* **2016**, *270*, 76–84.

(50) Jun, K. W.; Lee, H. S.; Roh, H. S.; Park, S. E. Catalytic Dehydration of Methanol to Dimethyl Ether (DME) over Solid-Acid Catalysts. *Bull. Korean Chem. Soc.* **2002**, *23* (6), 803–806.

(51) Sánchez-Contador, M.; Ateka, A.; Ibáñez, M.; Bilbao, J.; Aguayo, A. T. Influence of the Operating Conditions on the Behavior and Deactivation of a CuO-ZnO-ZrO_2@SAPO-11 Core-Shell-like Catalyst in the Direct Synthesis of DME. *Renew. Energy* **2019**, *138*, 585–597.

(52) Iliuta, I.; Larachi, F.; Fongarland, P. Dimethyl Ether Synthesis with in Situ H_2O Removal in Fixed-Bed Membrane Reactor: Model and Simulations. *Ind. Eng.*

Chem. Res. **2010**, *49* (15), 6870–6877.

(53) Diban, N.; Urtiaga, A. M.; Ortiz, I.; Ereña, J.; Bilbao, J.; Aguayo, A. T. Influence of the Membrane Properties on the Catalytic Production of Dimethyl Ether with in Situ Water Removal for the Successful Capture of CO_2. *Chem. Eng. J.* **2013**, *234*, 140–148.

(54) De Falco, M.; Capocelli, M.; Giannattasio, A. Membrane Reactor for One-Step DME Synthesis Process: Industrial Plant Simulation and Optimization. *J. CO2 Util.* **2017**, *22*, 33–43.

(55) Diban, N.; Aguayo, A. T.; Bilbao, J.; Urtiaga, A.; Ortiz, I. Membrane Reactors for in Situ Water Removal: A Review of Applications. *Ind. Eng. Chem. Res.* **2013**, *52* (31), 10342–10354.

(56) Rohde, M. P.; Unruh, D.; Schaub, G. Membrane Application in Fischer-Tropsch Synthesis to Enhance CO_2 Hydrogenation. *Ind. Eng. Chem. Res.* **2005**, *44* (25), 9653–9658.

(57) Rohde, M. P.; Schaub, G.; Khajavi, S.; Jansen, J. C.; Kapteijn, F. Fischer-Tropsch Synthesis with in Situ H_2O Removal - Directions of Membrane Development. *Microporous Mesoporous Mater.* **2008**, *115* (1–2), 123–136.

(58) Abashar, M. E. E.; Al-Rabiah, A. A. Investigation of the Efficiency of Sorption-Enhanced Methanol Synthesis Process in Circulating Fast Fluidized Bed Reactors. *Fuel Process. Technol.* **2018**, *179*, 387–398.

(59) Gorbe, J.; Lasobras, J.; Francés, E.; Herguido, J.; Menéndez, M.; Kumakiri, I.; Kita, H. Preliminary Study on the Feasibility of Using a Zeolite A Membrane in a Membrane Reactor for Methanol Production. *Sep. Purif. Technol.* **2018**, *200*, 164–168.

(60) Brunetti, A.; Drioli, E.; Barbieri, G. Energy and Mass Intensities in Hydrogen Upgrading by a Membrane Reactor. *Fuel Process. Technol.* **2014**, *118*, 278–286.

(61) Ateka, A.; Ereña, J.; Sánchez-Contador, M.; Perez-Uriarte, P.; Bilbao, J.; Aguayo, A. T. Capability of the Direct Dimethyl Ether Synthesis Process for the Conversion of Carbon Dioxide. *Appl. Sci.* **2018**, *8* (5), 677-691.

(62) Ateka, A.; Ereña, J.; Bilbao, J.; Aguayo, A. T. Kinetic Modeling of the Direct Synthesis of Dimethyl Ether over a CuO‑ZnO‑MnO/SAPO‑18 Catalyst and Assessment of the CO_2 Conversion. *Fuel Process. Technol.* **2018**, *181*, 233–243.

(63) Ateka, A.; Pérez-Uriarte, P.; Sierra, I.; Ereña, J.; Bilbao, J.; Aguayo, A. T. Regenerability of the CuO–ZnO–MnO/SAPO-18 Catalyst Used in the Synthesis of Dimethyl Ether in a Single Step. *React. Kinet. Mech. Catal.* **2016**, *119* (2), 655-670.

(64) Khajavi, S.; Kapteijn, F.; Jansen, J. C. Synthesis of Thin Defect-Free Hydroxy Sodalite Membranes: New Candidate for Activated Water Permeation. *J. Memb. Sci.* **2007**, *299* (1–2), 63–72.

(65) Khajavi, S.; Jansen, J. C.; Kapteijn, F. Application of Hydroxy Sodalite Films as Novel Water Selective Membranes. *J. Memb. Sci.* **2009**, *326* (1), 153–160.

(66) Khajavi, S.; Jansen, J. C.; Kapteijn, F. Performance of Hydroxy Sodalite Membranes as Absolute Water Selective Materials under Acidic and Basic Conditions. *J. Memb. Sci.* **2010**, *356* (1–2), 1–6.

(67) Khajavi, S.; Jansen, J. C.; Kapteijn, F. Application of a Sodalite Membrane Reactor in Esterification—Coupling Reaction and Separation. *Catal. Today* **2010**, *156* (3–4), 132–139.

(68) Stiefel, M.; Ahmad, R.; Arnold, U.; Döring, M. Direct Synthesis of Dimethyl Ether from Carbon-Monoxide-Rich Synthesis Gas: Influence of Dehydration Catalysts and Operating Conditions. *Fuel Process. Technol.* **2011**, *92* (8), 1466–1474.